Journal of Physics:
Condensed Matter

PAPER • **OPEN ACCESS**

Extraction of band gap energies and composition of mixed-phase polycrystalline semiconductors; a possible alternative method

To cite this article: H Idriss 2026 *J. Phys.: Condens. Matter* **38** 055001

Journal of Physics: Condensed Matter

OPEN ACCESS

RECEIVED
25 July 2025

REVISED
17 January 2026

ACCEPTED FOR PUBLICATION
23 January 2026

PUBLISHED
5 February 2026

PAPER

Extraction of band gap energies and composition of mixed-phase polycrystalline semiconductors; a possible alternative method

H Idriss*

Institute of Functional Interfaces (IFG), Karlsruhe Institute of Technology (KIT), 76344 Eggenstein-Leopoldshafen, Germany
Department of Chemistry, University College London, UCL, London WC1E 6BT, United Kingdom

* Author to whom any correspondence should be addressed.

E-mail: h.idriss@ucl.ac.uk

Keywords: band gap energy, titanium oxide anatase, titanium oxide rutile, Tauc plot, zinc oxide, carbon nitride

Supplementary material for this article is available online

Abstract

The optical band gap energy, E_g, of semiconductors is routinely determined using UV–Vis absorption measurements followed by Tauc-plot analysis. This method requires knowledge of the Tauc exponent n, which corresponds to the nature of the electronic transition. While Tauc analysis is effective for single-phase semiconductors, it may not be applicable to mixed-phase materials that exhibit two different types of transitions. In this work, the absorbance of mixed-phase TiO_2 (anatase and rutile) with varying compositions is examined. Anatase has an indirect band gap ($n = 2$), whereas rutile has a direct band gap ($n = 1/2$). It is shown that the first derivative of the absorbance with respect to the wavelength, $dA/d\lambda$, yields phase-composition information largely similar to that obtained from XRD analysis. Furthermore, the positive peak of the second derivative, $d^2A/d\lambda^2$, provides a band-gap value that does not shift (within <0.05 eV) with changes in TiO_2 phase composition. The method was also tested on two additional semiconductors (ZnO and g-C_3N_4), yielding band-gap energies comparable to those obtained using established techniques. These results demonstrate that the band gap energy can be determined without prior knowledge of the transition type by using the second derivative of the absorbance.

1. Introduction

Mixed-phase semiconductors have been used in many important technological applications for over a century. In photocatalysis they serve as interface junctions [1–5], enhancing charge separation and further driving excited electrons and holes transfer to different surface sites or to different surface terminations [6, 7], when possible. Knowledge of their optical band gap energies is therefore, routinely needed along with their composition. Computationally band gap energies of semiconductors can be extracted although usually with either hybrid methods (DFT + HF) or with the incorporation of the Hubard parameters (DFT + U) [8, 9]. This is because DFT underestimates the band gap energy. In general, experimentally the band gap energy of a semiconductor is extracted from UV–Vis absorbance measurements as a function of wavelength then by using the Tauc method [10, 11]. This method has received considerable attention and while it has its limitations when applied to crystalline materials it still offers a reliable estimate of the band gap energy for single semiconductor materials. Also, traditionally the phase composition is extracted from XRD patterns for crystalline semiconductors. The situation becomes more complex when two semiconductor phases are present with two different band gap energies, in particular when they have two different energy transitions (direct and indirect band gap energy, for example) such as in the case of the commonly used mixed phase TiO_2 (anatase and rutile). To explore this in some details a brief description is given below.

The Tauc equation is described as follows:

$$A^*\left(h\nu - E_g\right) = (\alpha h\nu)^{\frac{1}{n}} \quad (1)$$

where α is the absorption coefficient, which is a function of wavelength $\alpha(\lambda)$, h is Planck constant, E_g is the optical band gap of the semiconductor, ν is incident light frequency, A^* is a constant, and n is the Tauc exponent. n may have different values depending on the type of energy transition. Generally, it is recommended to use A^* instead of A based on previous comprehensive work by others [12]. In particular, $n = 1/2$ for direct (allowed) transitions and $n = 2$ for indirect (allowed) transition are used. In practice, a plot of $(\alpha h\nu)^{1/n}$ as a function of $h\nu$ is made and extrapolation of the linear range beyond the absorption edge yields the value of E_g on the abscissa axis and for that the value of n needs to be known [13]. Also, as clearly presented in earlier studies, the constant (A^*) is sensitive to the presence of defects, known as Urbach tail absorption [14]. The derivative of the Tauc equation gives the slope A^*,

$$\left[\frac{\mathrm{d}(\alpha h\nu)^2}{\mathrm{d}(h\nu)}\right]_{h\nu=E_g} = A^* = B^2 {E_g}^2 \tag{2}$$

where B is a factor as defined by equation (12) in [12].

In previous work, an evaluation of B [12] was conducted in the case of ZnO (another wide band gap semiconductor with a (direct) band gap energy at room temperature of ca. 3.3 eV) [15]. The theoretical value of B for ZnO is equal to 3×10^{12}. Based on 73 plots the authors [12] found that while the mean B did not deviate by much its values ranged from 10^7 to 10^{16}. One of the main reasons for the deviations is related to the absorption coefficient, α.

As pointed out [16], for example in the case of a direct transition, α is equal to

$$\alpha_{\mathrm{dir}}\left(E < E_g\right) = 0 \text{ and } \alpha_{\mathrm{dir}}\left(E \geqslant E_g\right) \propto \left(E - E_g\right)^{\frac{1}{2}} \tag{3}$$

and the following assumptions are made. (1) No Coulomb attraction between the e-h generated pairs, (2) the absence of extrinsic absorption often due to defect states and impurities, and (3) the fact that the parabolic-like shape of $\alpha_{\mathrm{dir}}\left(E \geqslant E_g\right)$ is valid only at electron wave-vector, $\vec{k} = 0$.

When the semiconductor analyzed has an indirect electronic transition α changes.

$$\alpha_{\mathrm{indir}}\left(E \geqslant E_g\right) \propto \left(E \pm h\Omega - E_g\right)^2 \tag{4}$$

where $h\Omega$ is the phonon emitted $(-)$ or absorbed $(+)$. It is therefore obvious that a Tauc plot for mixed phases requires two values of n. If in addition the phase composition is not known the contribution of each phase in the plot cannot be determined.

An alternative method that has been in practice in solution chemistry to evaluate the absorption energy, where two or more light absorbing substances are present, is to use the derivatives of the absorbance replotted as a function of the wavelength [17, 18]. Actually, derivative spectroscopy has been used for over a century and can provide considerable information on the absorption bands [19, 20]. The idea behind it rests upon the measurement of the first or higher derivatives of the absorbance, A, with respect to the wavelength, $\mathrm{d}A/\mathrm{d}\lambda$, $\mathrm{d}^2A/\mathrm{d}\lambda^2$, etc. One of the advantages lies in its capability to resolve or enhance weak absorbance related to a small concentration of a given compound when compared to the other. This method has in some cases been used to analyze solid materials, although not for a direct extraction of the band gap energy. For example, the first derivative [21] $(\mathrm{d}A/\mathrm{d}\lambda)$ was used to further study the absorbance of TiO_2. The second derivative $(\mathrm{d}^2A/\mathrm{d}\lambda^2)$ method was also used to identify changes of the absorbance of solid $Pb_{1-x}Sr_xSe$, where the band gap energy transition changes from direct to indirect [22] as a function of the concentration of Sr. Also, in a work on CdSe quantum dots [23], a close matching of the transition energies with the second derivative of the absorption spectra was observed and was suggested as a method to provide the electronic transition energy.

Putting the above together one may point out that extraction of the band gap energies of a mixed phase wide band gap oxide semiconductor, in particular if it contains some oxygen defects (like most n-type semiconductors), might be obtained using derivative spectroscopy instead of, or in addition to, the traditional Tauc plot method. In this work, the extraction of the band gap energies of a mixed phase oxide with different compositions of samples based on TiO_2 anatase and rutile with different relative compositions, have been evaluated by diffused reflectance spectroscopy (DRS) and XRD diffraction. The objective is to test the possibility of extracting both the band gap energies and phase composition from one measurement (UV–vis) without the needed knowledge of the nature of the optical transition (direct (TiO_2 rutile) or indirect (TiO_2 anatase)).

2. Methodology

TiO_2 (anatase) (Hombikat by Sachtleben Chemie GmbH) was used as the starting oxide. The powder XRD pattern was collected using a Panalytical Empyrean series 2-XRD at the following condition: A 2θ range between 5 and 90° was used with a step size of 0.013° and a step time of 0.1 s. The x-ray, Ni-filtered Cu Kα radiation source ($\lambda_{K\alpha}$ = 1.5418 Å) was operated at 45 mA and 40 kV.

UV–vis absorbance spectra of the powder samples were collected over the wavelength range of 250–900 nm (1 nm/step) using a Thermo Fisher Scientific UV–vis spectrophotometer equipped with praying mantis diffuse reflectance (R) accessory. The following relational expression is used for the determination of the band gap energy; $(h\nu\alpha)^{1/n} = A(h\nu - E_g)$. Where h: Planck's constant, ν: frequency of vibration, α: absorption coefficient, E_g: band gap energy, A: proportional constant. The value of the exponent n denotes the nature of the transition. The obtained diffuse reflectance spectra are converted to Kubelka–Munk function ($F(R) = (1-R)^2/2R$), where R is reflectance. The vertical axis is converted to quantity $F(R_\infty)$, which is proportional to the absorption coefficient. The α in the Tauc equation is substituted with $F(R_\infty)$. Then, the expression becomes $(h\nu F(R_\infty))^{1/n} = A(h\nu - E_g)$. A fraction fit line (20%–70%) is drawn tangent to the point of inflection on the curve of the function and the $h\nu$ value at the point of intersection of the tangent line and the horizontal axis is the band gap E_g value.

TiO_2 (anatase) sample were heated in a furnace (in air) at different temperatures to transform part or all of the anatase phase to rutile as depicted in figure S1. Evaluation of the phase composition of anatase (A) and rutile (B) using XRD was conducted using the following formula [24]:

$$\%\, R = \frac{1}{\left[\left(\frac{A}{R}\right) \times 0.884 + 1\right]} \times 100. \tag{5}$$

It was further checked with a Rietveld refinement type method, as follows.

1. Each diffraction pattern was imported into a uniform numerical format (2θ vs. intensity). A smooth background was approximated using a quadratic polynomial and subtracted before refinement to remove instrumental and fluorescence contributions. No artificial smoothing or intensity normalization was applied prior to fitting.
2. Phase identification: all patterns corresponded to TiO_2 in either the anatase (tetragonal, space group $I4_1/amd$) or rutile (tetragonal, space group $P4_2/mnm$) polymorphs.
3. Rietveld-type refinement procedure: quantitative phase analysis was performed using a custom Rietveld-type whole-pattern least-squares routine implemented in Python. The method models the experimental intensity $I_{obs}(2\theta)$ as a sum of phase contributions plus background.
4. Each Bragg peak position $2\theta\_(hkl)$ is calculated from Bragg's law using the refined lattice parameters a and c: $\frac{1}{d^2} = \frac{h^2+k^2}{a^2} + \frac{l^2}{c^2}$, $2\theta = 2\sin^{-1}\left(\frac{\lambda}{2d}\right)$
5. Peak-shape function: a pseudo-Voigt (PV) function (a symmetric mixture of Gaussian and Lorentzian shapes) was used to describe peak profiles. The full width at half maximum (FWHM), β, was modeled as:
   $\beta^2 = \left(\frac{K\lambda}{D\cos\theta}\right)^2 + (4 \in \tan\theta)^2$ [2] where K = shape factor (0.9), D = apparent crystallite size, ε = microstrain (dimensionless), and θ = Bragg angle.
6. Parameters refined: for each pattern, the following parameters were refined simultaneously by non-linear least squares (Levenberg–Marquardt algorithm): phase scale factors: $S_{anatase}$, S_{rutile}; lattice constants: $a_{anatase}$, $c_{anatase}$, a_{rutile}, c_{rutile}; instrumental/geometry: zero-shift ($\Delta 2\theta$); microstructural: apparent crystallite size (D), microstrain (ε); background: quadratic polynomial coefficients (b_0, b_1, b_2).
7. Goodness of fit: the refinement quality was evaluated using standard Rietveld reliability factors:
   R_{wp}; Rp and χ^2.
8. Weight fractions of anatase and rutile were obtained from normalized scale factors:

$$W_{anatase} = \frac{S_{anatase}}{S_{anatase} + S_{rutile}} \times 100,\ W_{rutile} = 100 - W_{anatase}.$$

The crystallite sizes were cross checked by the Scherrer equation; the values are reported in table 1. All analyses were implemented in Phyton (v3.11) using least square optimization routine.

ZnO–NaOH was synthesized by precipitation in aqueous methanol solution. Briefly, 1.98 g zinc acetate dihydrate (Sigma Aldrich, > 98%) was mixed with 40 ml of methanol (Sigma Aldrich, HPLC Grade > 99%) and refluxed at 64 °C for 5–6 min. De-Ionized water (18.2 MΩ) was added dropwise to the solution followed by the addition of 30 ml of 0.7 M NaOH in methanol dropwise. The solution was then left to reflux at 64 °C for additional 30 min. The white precipitate was then collected by centrifuging at 6500 rpm for 15 min. The precipitate was washed with 1:1 ethanol: acetone solution 3 times and stored in a vacuum desiccator overnight. This was followed by calcination at 400 °C for two hours with a ramping rate of 10 °C mim^{-1}.

C_3N_4 was synthesized directly from melamine (99% Sigma Aldrich) via a solid-state thermal polycondensation reaction procedure. The white precursor was heated at 600 °C for 15 h in static air (i.e. heating rate: 5 °C min^{-1}) in an alumina crucible covered with aluminum foil.

3. Results and discussion

Before making a comparison between the optical spectra of the mixed phases, it is opted to first present the absorbance of a single phase. In this case there are no obvious issues and extraction of the optical band gap energy is relatively straight forward. This is presented in figure 1 in which the absorbance as a function of wavelength of a polycrystalline TiO_2 anatase powder is plotted (figure 1(A)) along with the corresponding Tauc plot [25] in figure 1(B). The XRD pattern of TiO_2 anatase and the other TiO_2 powders used in this work are presented in figure S1.

While TiO_2 Hombikat is pure anatase (see figure S1), it is opted to heat it to the highest possible temperature (900 °C, just before the appearance of the rutile phase) in order to obtain a reasonably pure crystalline anatase phase. The crystallite size of this anatase phase was calculated to be equal to 43 nm. Both plots give very close results. The asymptote of the absorbance intersection with the x-axis gives a band gap energy of 3.27 eV (380 nm) which matched the value obtained from the Tauc plot. It is noted that the baseline goes to near zero in both plots and therefore the extrapolation is unlikely to have errors. In figure 1(A) the first derivative of the absorbance (A) with respect to λ is indicated at about the inflection point. Also shown is the second derivate at the bottom curvature. An arrow indicates an approximate position pointing to intersection with the x-axis at the same position as the asymptote intersection. This is more detailed in figure 2 for the series studied.

Figure 2 presents absorbance spectra, along with their first and second derivatives, for TiO_2 100% anatase and of TiO_2 100% rutile with respect to λ. The shift to a higher wavelength (lower energy) of the rutile absorbance is clear. The weak increase in absorbance just above the band edge in rutile TiO_2 (between ∼3.0 and 3.8 eV) arises from the onset of weakly allowed transitions. These may originate both from deeper valence-band states to the conduction-band minimum, and from valence-band maximum electrons to higher-lying conduction-band states. This behavior is consistent with the electronic structure of rutile [21], where the fundamental direct transition is dipole-forbidden and strong dipole-allowed transitions occur only above ∼4 eV. It is however observed that the baseline does not go to zero in the case of the rutile and there is some absorption between about 400 and 600 nm (attributed to oxygen defects [26] among others and the unavoidable formation of the Magneli phase [27]). The Tauc plots of the two samples are presented in figure S2.

Figure 2(B) presents the first derivative (for a better display it is presented as $-dA/d\lambda$, so the peaks are positive). The baseline is much better for the TiO_2 and would unlikely affect the band widths for both samples. The negative peak on the low wavelength side is due to the increased absorption as seen in the absorbance spectra of figure 2(A). It is to be noted that the FWHM of the TiO_2 rutile (22–23 nm) is smaller than that of the anatase (30 nm) sample. The density of states of the anatase and rutile bulk structures is largely similar therefore this is unlikely to be due to differences in possible available filled states (at the valence band) or empty states (in the conduction band) [28]. The difference may be due to higher crystallinity of the rutile sample compared to the anatase one. It has been reported that the presence of less crystalline phases in TiO_2 leads to higher density of localized states near the band edges [29]. These are often referred to as 'tail states' related to structural disorder (due to the displacement of O atoms from the plane containing three neighboring Ti atoms), which are largely absent or much less pronounced in highly crystalline phases.

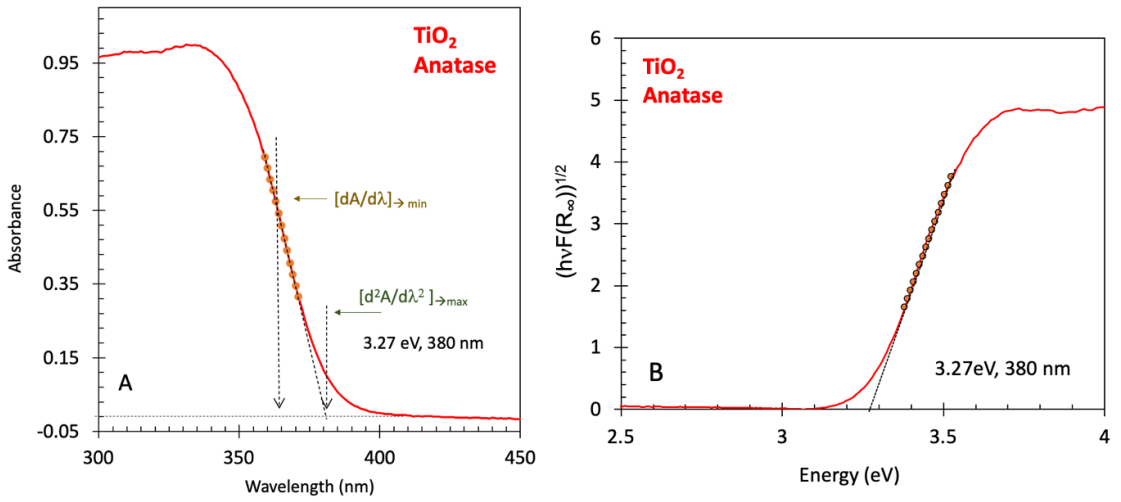

Figure 1. Absorbance spectrum of TiO_2 anatase of ca. 40 nm crystallite size (see figure S1 for XRD patterns). (A). As recorded absorbance spectrum, (B). Tauc plot of the data in (A) in which the Kubelka–Munk function $F(R_\infty)$ replaces the absorption coefficient; see methodology section. The dot points in (A) and (B) are linear regressions.

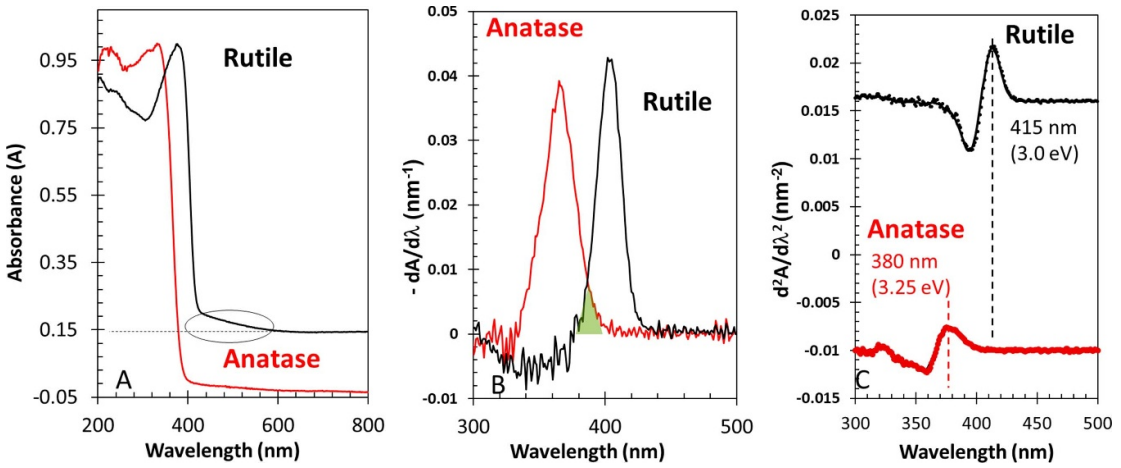

Figure 2. (A) Absorbance as a function of wavelength plots for 100% anatase and 100% rutile TiO_2 (see figure S1 for XRD of the samples); note the finite absorption or tail below the band gap is highlighted and attributed to bulk defects. (B) Negative of the first derivative, $dA/d\lambda$, with respect to λ, of the data in (A); note that the rutile $dA/d\lambda$ is sharper than that of the anatase TiO_2. (C) Second derivative with respect to λ, $d^2A/d\lambda^2$, of the data in (A); the vertical dashed lines point to the peak maxima which coincides with the values of the band gap energies. The green triangle in (B) highlight the energy overlap between anatase and rutile phases; the raw data are points and the lines corresponds to 5-point smoothed fit.

Another observation is the presence of an overlap of $dA/d\lambda$ between both phases as highlighted in figure 2(B). Its meaning is not clear, although it is worth mentioning as indicated in equation (2) that the derivative of the Tauc equation gives A^* which is sensitive to defects (Urbach tail).

The second derivative is presented in figure 2(C). The maximum of the positive peak for each sample, that is at the high energy side of curvature of the absorbance is equal to 415 nm (3.0 eV) for rutile phase and 380 nm (3.25 eV) for the anatase phase. While these numbers are very close to those obtained from the asymptotes, they have the merit of being insensitive to the way they are drawn because each originates from a single point, and there was no need to invoke the nature of the electronic transition. There are two curvatures in a typical absorbance spectrum of a semiconductor, such as that presented in figure 1(A). These are captured by the second derivatives. The first is negative and below the middle of the absorbance. This is the region of deeper valence band electrons while the second (positive) after the middle of the absorbance originates from electrons statistically close to the upper edge of the valence band. It is found that this corresponds to values obtained either upon direct extraction from a linear fit of the region of concern of the absorbance plot or upon using the Tauc plot.

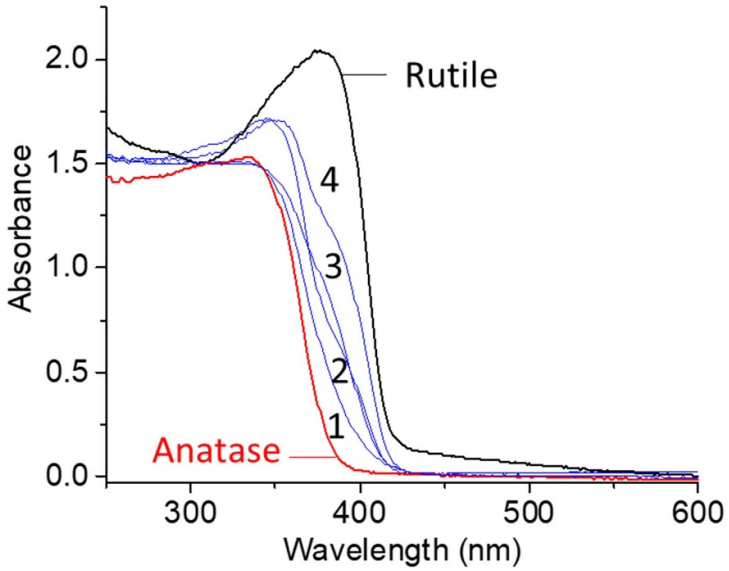

Figure 3. Diffused reflectance spectroscopy (DRS) of a series of TiO_2 powders containing anatase and/or rutile phases. Samples labeled 1–4 contain both phases. See table 1 and figures S1 and S3 for further information on the structure and fraction of the two phases in the samples.

To further see the merit of this method figure 3 presents the series of samples in which both TiO_2 phases are present. In this case, both electron transitions occur (direct for rutile, $n = 1/2$, and indirect of anatase, $n = 2$). Changes in the slope of the absorbance with wavelength due to the increasing presence of the rutile phase is clear.

Figure 4(A) presents the negative of the first derivative. The presence of the two phases gives rise to two distinct peaks. Fitting was conducted by taking the parameters from pure anatase and pure rutile as seen in the bottom and top spectra. The relative peak areas attributed to the anatase and rutile phases are given in table 1 together with those obtained from XRD. It is found that the fraction of each phase obtained from $dA/d\lambda$ plots is similar to that obtained from XRD. The slight changes are attributed to deviations in fitting the peaks in the derivative plots as well as to deviations of the composition obtained from XRD. Figure 4(B) shows the plots of the second derivative, $d^2A/d\lambda^2$. Pure anatase and rutile have one negative and one positive peak. The positive peaks maxima are now used to point to the position of the band gap energies of the mixed phases. In the case of the mixed phases the plots contain four peaks, two negative and two positive peaks. The extracted band gap energies are given in table 1 and deviated by <0.05 eV which is within experimental and analytical errors.

It therefore appears that one can extract both the phase composition and band gap energy of mixed polycrystalline oxide phases using the DRS data alone and without the need to include the nature of the electronic transition. It is also worth mentioning that the values of the extracted band gap energies did not change with composition, most likely because the separation of about 30 nm between the two phases is large enough to prevent overlaps.

The fact that the method works well in the case of polycrystalline TiO_2 might be because of combination of a few factors, in particular because the energy separation is relatively large (0.2 eV difference $\approx$ 30 nm). For other mixed phases with smaller band gap energies differences, data acquisition will need to be conducted with smaller steps ($\Delta\lambda$).

The correspondence between the XRD results and the first derivative is made possible because of the crystallinity of the samples and is shown as a guide. Moreover, the first derivative method to extract the contribution of both phases might be useful for estimation of their relative contributions, if they are less crystalline, where in this case extraction of their composition by XRD is not simple. Further work needs to be conducted on other semiconductors in order to validate such a correspondence.

4. Other semiconductors

While successful extraction of the phase contributions from the first derivative is clear (as it in line with those obtained from XRD), the extraction of the band gap energy from the second derivative will benefit from comparison with other semiconductors. It is beyond the present work to conduct extensive measurements on many other semiconductors. However, figure 5 presents two other semiconductors

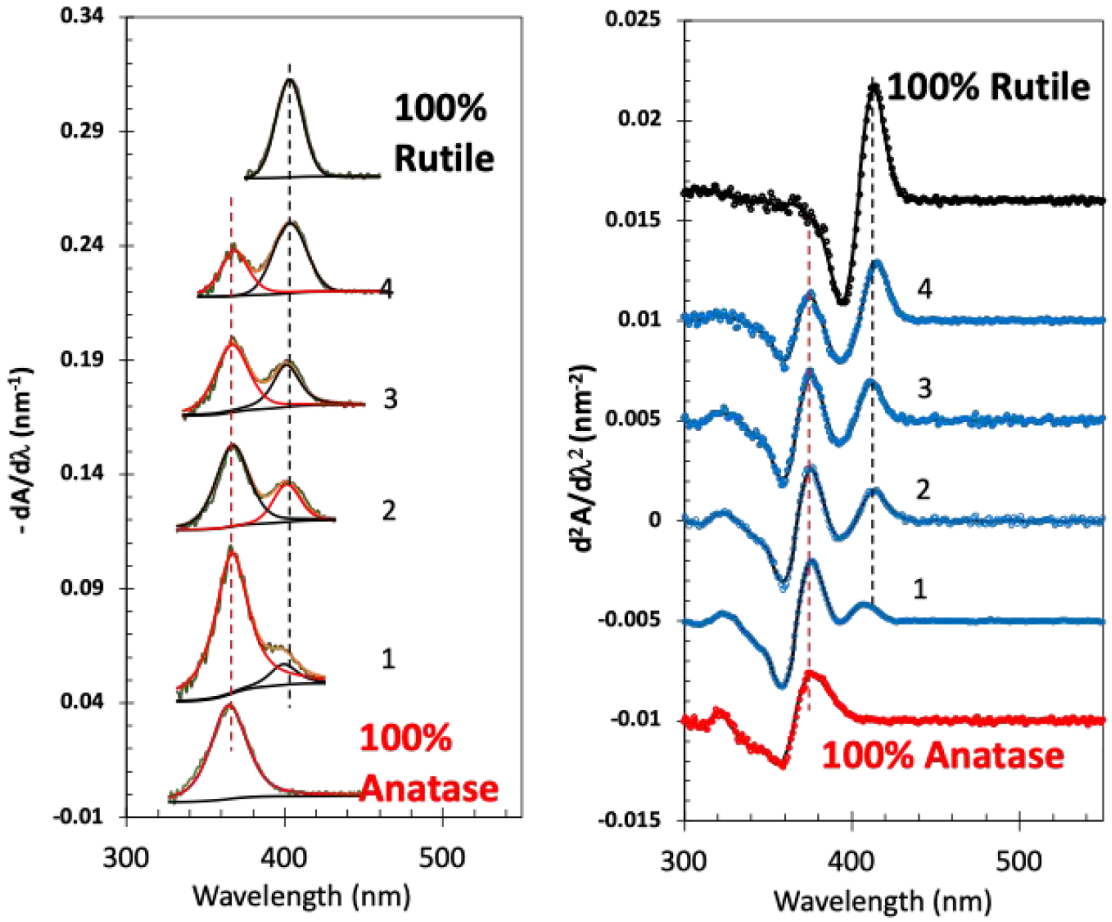

Figure 4. (A) Negative of the first derivative, $dA/d\lambda$, with respect to λ, of the data in figure 3. (B) Second derivative with respect to λ, $d^2A/d\lambda^2$, of the data in figure 3; the vertical dashed lines point to the peak maxima which coincides with the values of the band gap energies (see table 1); the raw data are points and the lines corresponds to five-point smoothed fit.

Table 1. Fractions of the rutile phase as obtained from XRD patterns and from the first derivative of the absorbance (using DRS) $dA/d\lambda$). Also shown are the crystallite sizes obtained from XRD and the band gap energy obtained from the second derivative, $d^2A/d\lambda^2$.

Sample	Rutile fraction XRD[a]-(101)A/(101)R	Rutile fraction XRD[b]- Rietveld refinement	Rutile fraction, using $dA/d\lambda$ plots (UV vis.)	Crystallite size Anatase/Rutile	Anatase, E_g using ($d^2A/d\lambda^2$) nm (eV)	Rutile, E_g using ($d^2A/d\lambda^2$) nm (eV)
100% anatase	0	0	0	43 nm /—	380 (3.26)	—
1	0.08	0.10	0.09	45 nm /—	378 (3.28)	411 (3.01)
2	0.23	0.20	0.25	48 nm/45 nm	378 (3.28)	415 (2.99)
3	0.31	0.35	0.35	47 nm/43 nm	377 (3.29)	413 (3.00)
4	0.67	0.55	0.60	48 nm/48 nm	377 (3.29)	416 (2.98)
100% rutile	1	1	1	-/51 nm	—	415 (2.99)

[a] See equation (5).

[b] See methodology section and figure S3. The errors of the fractional numbers of rutile are about ±10%.

that give relatively clear absorbance in the UV and visible regions: ZnO (direct band gap) and C_3N_4 (indirect band gap), respectively. The ZnO sample analyzed has recently been studied in more detail by pump probe femto-second transient absorption spectroscopy (TAS) in addition to XRD, TEM and DRS. It is highly crystalline with lattice parameters matching standard wurtzite ZnO reference samples [30]. Comparison between its ground state bleaching as monitored by TAS and the first derivative of its absorbance as obtained from DRS indicated considerable similarities. Most important, the first derivative peak had the narrowest FWHM of the three ZnO samples studied which together with the narrowest XRD peaks further point to a possible relation related to the degree of crystallinity. The second derivative plot gives a band gap energy of 3.27 eV. Extraction of its band gap energy using the Tauc method

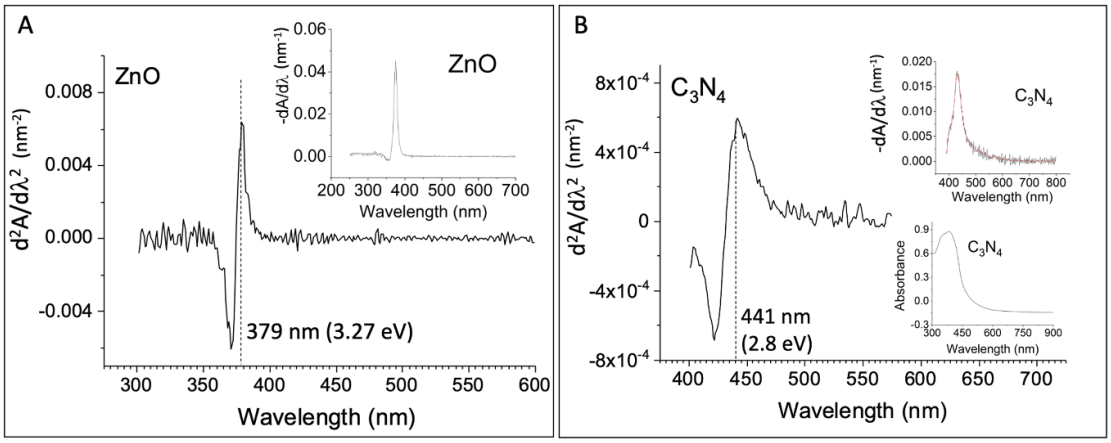

Figure 5. (A) First (inset) and second derivatives of the absorbance with respect to the wavelength for a polycrystalline ZnO sample. (B) Absorbance, its first derivative (both as insets) and its second derivative with respect the wavelength of C_3N_4 that was prepared from melamine.

gave a very close band gap energy (3.24 eV). This is similar to other ZnO samples in different forms where a band gap energy of 3.3 eV is taken as the standard [31].

Figure 5(B) shows the absorbance, $dA/d\lambda$ and $d^2A/d\lambda^2$ of a C_3N_4 sample. While considerable work is devoted to its properties it is an emerging material and still some of its properties not well understood. Previous work has shown that C_3N_4 prepared from melamine is crystalline [32]. This sample is part of a series that was studied by several methods including XRD, TEM, DRS and XPS core and valence levels. Its band gap energy varied as a function of calcination temperature, with the sample calcined at 600 °C having the lowest E_g (extracted from the Tauc plot) and that was found to be 2.7–2.8 eV. The one extracted from the second derivative in figure 5(B), gave an E_g of 2.80 eV. The proposed method might be able to separate 2D from g-C_3N_4 since the former has a band gap energy about 0.2 eV larger than the latter [33, 34]. The Tauc plots of ZnO and C_3N_4 are presented in figure S4.

4.1. Potential and limitations of second-derivative and Tauc-based approaches for band-gap determination

The determination of semiconductor band-gap energies from UV–Vis diffuse reflectance spectroscopy (DRS) remains a widely used method-dependent procedure. Graphical approaches analyses are particularly sensitive to the quality of the experimental data, including baseline stability, signal-to-noise ratio, scattering effects, and phase purity. Small variations in data preprocessing or in the selected fitting window can lead to substantial differences in the extracted band-gap energy. A recent methodological investigation demonstrated that band-gap values derived from identical DRS datasets may differ by up to 0.8–0.9 eV depending on the evaluation method employed, particularly for mixed-phase or doped TiO_2 systems [35]. This sensitivity is especially pronounced for materials exhibiting multiple optical transitions, such as mixed anatase–rutile TiO_2 or doped TiO_2, where the Tauc method may yield an apparent band-gap that reflects the dominant absorption feature rather than the fundamental transition. Several studies have reported significant band-gap shifts derived from Tauc plots in such systems, even when structural characterization indicates only modest changes in phase composition or defect density [36–38]. This illustrates that Tauc-based band-gap values need to be interpreted with caution, particularly when comparing materials with different morphologies, dopant concentrations, or phase mixtures. As seen in figure 4(B), the maximum of the second derivative positive peak is largely not sensitive to phase composition. Also, one notices that the stability of the base line of the spectra. Probably the most important point is that when two phases of the same semiconductor are present, each having a different electronic transitions, n, the Tauc equation cannot be applied.

Derivative-based methods offer further insight. While the first-derivative approach often identifies inflection points located above the true band edge and therefore overestimate the band-gap energy [39], it is useful for distinguishing multiple absorption onsets and, consequently, different phases, as shown in this work, with different electronic transitions within the same material. The second-derivative method emphasizes subtle changes in absorption curvature and enables a more direct identification of band-edge transitions, reducing subjectivity associated with the selection of linear fitting regions.

The applicability of these methods also depends on the dimensionality of the material. For layered or two-dimensional systems such as graphitic carbon nitride (g-C_3N_4), quantum confinement effects [40],

altered density of states near the band edges, and enhanced excitonic contributions may invalidate the assumptions underlying conventional Tauc analysis, which is derived for bulk semiconductors with parabolic band dispersions. Consequently, band-gap values obtained from Tauc plots for two-dimensional g-C_3N_4 nanosheets should be regarded as effective optical gaps rather than strict electronic band gaps. In this context, derivative-based approaches provide a more robust comparative tool for identifying relative shifts in absorption onset and phase-related features.

Overall, while graphical methods based on UV–Vis DRS remain valuable for comparative analysis, their limitations must be acknowledged. Combining derivative-based techniques with structural and spectroscopic characterization is still needed for reliable interpretation of optical transitions, particularly in complex, mixed-phase, doped, or low-dimensional semiconductor systems.

5. Conclusions

The absorbance of TiO_2 samples containing different proportions of anatase and rutile phases was studied in this work in order to directly obtain their band gap energies without the need to use Tauc plots. This is because the Tauc method requires the use of n (the energy transition) in a single plot and this is not possible when two phases are present in a given semiconductor. Anatase has an indirect band gap energy ($n = 2$) and rutile has a direct band gap energy ($n = 1/2$).

The first derivative of the absorbance ($dA/d\lambda$) was found to provide a phase-composition largely similar to that obtained from XRD analysis. Furthermore, the positive peak of the second derivative, $d^2A/d\lambda^2$, yielded band gap energies for both phases when present simultaneously, and these values that did not shift with changes in phase composition.

Additional semiconductors were also examined (ZnO and g-C_3N_4), and their band gap energies were successfully extracted using the second derivative approach.

Overall, the second derivative method, offers a practical means of estimating the band gap energy without prior knowledge of whether the transition is direct or indirect. This approach is therefore particularly useful for mixed-phase semiconductors, where an estimate of the phase composition and extraction of the band gap energy can be obtained from the same UV–Vis measurement.

Data availability statement

All data that support the findings of this study are included within the article (and any supplementary files).

Properties of mixed phase TiO_2 available at https://doi.org/10.1088/1361-648X/ae3cf5/data1.

Acknowledgments

The authors acknowledge the contribution of Dr K. Wahab (then at SABIC research center at KAUST) who prepared and analyzed the TiO_2 samples by DRS and XRD methods and Mr. M. Aloufi (at SABIC research center at KAUST) who prepared and analyzed the C_3N_4 sample. The author thanks Professor Geoff Waterhouse (Department of Chemistry, University of Auckland, New Zealand), Dr Amtiaz Nadeem (SABIC research center at KAUST, Saudi Arabia), Dr Jeremy Bao (Catalysis Center, KAUST, Saudi Arabia) and Dr Vedran Jovic (GNS, CRI, Gracefield, New Zealand) for providing their opinions and critical examination of the work.

Author contribution

H Idriss 0000-0001-8614-7019

Conceptualization (equal), Formal analysis (equal), Investigation (equal), Resources (equal), Software (equal), Validation (equal), Writing – original draft (equal), Writing – review & editing (equal)

References

[1] Zhang X, Lin Y, He D, Zhang J, Fan Z and Xie T 2011 Interface junction at anatase/rutile in mixed-phase TiO_2: formation and photo-generated charge carriers properties *Chem. Phys. Lett.* **504** 71–75

[2] Bashir S, Wahab A K and Idriss H 2015 Synergism and photocatalytic water splitting to hydrogen over M/TiO_2 catalysts: effect of initial particle size of TiO_2 *Catal. Today* **240** 242–7

[3] Wahab A K, Ould-Chikh S, Meyer K and Idriss H 2017 On the 'possible' synergism of the different phases of TiO_2 in photocatalysis for hydrogen production *J. Catal.* **352** 657–71

[4] Sinatra L, LaGrow A P, Peng W, Kirmani A R, Amassian A, Idriss H and Bakr O M 2015 A Au/Cu_2O–TiO_2 system for photocatalytic hydrogen production. A pn-junction effect or a simple case of *in situ* reduction? *J. Catal.* **322** 109–17

[5] Schulte K L, DeSario P A and Gray K A 2010 Effect of crystal phase composition on the reductive and oxidative abilities of TiO_2 nanotubes under UV and visible light *Appl. Catal. B* **97** 354–60
[6] Zhang J, Wang X, Wang X and Li C 2025 Heterophase junction effect on photogenerated charge separation in photocatalysis and photoelectrocatalysis *Acc. Chem. Res.* **58** 787–98
[7] Wang X and Li C 2018 Roles of phase junction in photocatalysis and photoelectrocatalysis *J. Phys. Chem. C* **122** 21083–96
[8] Alghamdi H and Idriss H 2018 Study of the modes of adsorption and electronic structure of hydrogen peroxide and ethanol over TiO_2 rutile (110) surface within the context of water splitting *Surf. Sci.* **669** 103–13
[9] Bashyal K, Pyles C K, Afroosheh S, Lamichhane A and Zayak A T 2018 Empirical optimization of DFT + U and HSE for the band structure of ZnO *J. Phys.* **30** 065501
[10] Makuła P, Pacia M and Macyk W 2018 How to correctly determine the band gap energy of modified semiconductor photocatalysts based on UV−Vis spectra *J. Phys. Chem. Lett.* **9** 6814–7
[11] Tauc J, Grigorovici R and Vancu A 1966 Optical properties and electronic structure of amorphous germanium *Phys. Status Solidi b* **15** 627–37
[12] Coulter J B and Birnie D P III 2018 Assessing Tauc plot slope quantification: ZnO thin films as a model system *Phys. Status Solidi b* **255** 1700393
[13] Haryński Ł, Olejnik A, Grochowska K and Siuzdak K 2022 A facile method for Tauc exponent and corresponding electronic transitions determination in semiconductors directly from UV–Vis spectroscopy data *Opt. Mater.* **127** 112205
[14] Urback F 1953 The long-wavelength edge of photographic sensitivity and of the electronic absorption of solids *Phys. Rev.* **92** 1324
[15] Ziani A, Al-Taweel S, Nadeem M A and Idriss H 2022 Effect of gold loading on time-resolved ps photoluminescence of ZnO *J. Phys. Chem. C* **126** 16148–57
[16] Zanatta A R 2019 Revisiting the optical bandgap of semiconductors and the proposal of a unified methodology to its determination *Sci. Rep.* **9** 11225
[17] Dixit L and Ram S 1985 Quantitative analysis by derivative electronic spectroscopy *Appl. Spectrosc. Rev.* **21** 311–418
[18] Owen A J Uses of derivative spectroscopy *Application Note* (available at: www.youngin.com/application/an-0608-0115en.pdf)
[19] Daymond E G 1923–25 *Proc. Camb. Phil. Soc.* **22** 405
[20] Giese A T and French C S 1955 The analysis of overlapping spectral absorption bands by derivative spectrophotometry *Appl. Spectrosc.* **9** 78–96
[21] Diamantopoulos N C, Barnasas A, Garoufalis C S, Anyfantis D, Bouropoulos N, Poulopoulos P and Baskoutas S 2020 Band gap measurements of nano-meter sized rutile thin films *Nanomaterials* **10** 2379
[22] Ravindra N M, Ganapathy P and Choi J 2007 Energy gap–refractive index relations in semiconductors—an overview *Infrared Phys. Technol.* **50** 21–29
[23] Thupakula U, Khan A H, Bal J K, Ariga K and Acharya S 2011 Size selective excitonic transition energies in strongly confined CdSe quantum dots *J. Nanosci. Nanotechnol.* **11** 7709–14
[24] Xianzhi F, Clark L A, Yang Q and Anderson M A 1996 Enhanced photocatalytic performance of titania-based binary metal oxides: TiO_2/SiO_2 and TiO_2/ZrO_2 *Environ. Sci. Technol.* **30** 647–53
[25] Kubelka P and Munk F 1931 Ein beitrag zur optik der farbanstriche *Z. Tech. Phys.* **12** 593–601
[26] Llansola-Portoles M J, Bergkamp J J, Finkelstein-Shapiro D, Sherman B D, Kodis G, Dimitrijevic N M, Gust D, Moore T A and Moore A L 2014 Controlling surface defects and photophysics in TiO_2 nanoparticles *J. Phys. Chem. A* **118** 10631–8
[27] Zhang Q *et al* 2021 Z. Andersson-Magnéli phases Ti_nO_{2n-1}: recent progress inspired by Swedish scientists *Z. Anorg. Allg. Chem.* **647** 126–33
[28] Labat F, Baranek P and Adamo C 2008 Structural and electronic properties of selected rutile and anatase TiO_2 surfaces: an ab initio investigation *J. Chem. Theory Comput.* **4** 341–52
[29] Prasai B, Cai B, Underwood M K, Lewis J P and Drabold D A 2012 Properties of amorphous and crystalline titanium dioxide from first principles *J. Mater. Sci.* **47** 7515–21
[30] Alamoudi M, Alrushaid M, Nadeem A M, Katsiev K and Idriss H 2025 Charge carrier dynamics of polycrystalline ZnO. Comparing ground state bleaching to ground state absorption *J. Phys. Chem. C* **129** 14565–75
[31] Özgür Ü, Alivov Y I, Liu C, Teke A, Reshchikov M A, Doğan S, Avrutin V, Cho S-J and Morkoç H 2005 A comprehensive review of ZnO materials and devices *J. Appl. Phys.* **98** 041301
[32] Caux M, Fina F, Irvine J T S, Idriss H and Howe R 2017 Impact of the annealing temperature on Pt/g-C_3N_4 structure, activity and selectivity between photodegradation and water splitting *Catal. Today* **287** 182–8
[33] Moadelli M and Badehian H A 2023 Reduced band gap in 2D-C_3N_4 nanosheets decorated with silver and gold adatoms *Phys. Scr.* **98** 125901
[34] Yuana Y-J *et al* 2019 Liquid exfoliation of g-C_3N_4 nanosheets to construct 2D-2D MoS_2/ g-C_3N_4 T photocatalyst for enhanced photocatalytic H_2 production activity *Appl. Catal. B* **246** 120–8
[35] Welter E S, Garg S, Gläser R, M and Goepel M 2023 Methodological investigation of the band gap determination of solid semiconductors via UV/Vis spectroscopy *ChemPhotoChem* **7** e202300001
[36] Apopei P, Catrinescu C, Teodosiu C and Royer S 2014 Mixed-phase TiO_2 photocatalysts: crystalline phase isolation and reconstruction, characterization and photocatalytic activity in the oxidation of 4-chlorophenol from aqueous effluents *Appl. Catal. B* **160–161** 374–82
[37] Draoui A, Hebboul Z, Boudabia S, Lefkaier I B, Naidjate M E, Belbel A, Aroudji H, Mokhtari A and Goumri-Said S 2025 Cost-effective transformation of rutile to anatase and synthesis of $Zn_2Ti_3O_8$ *Chem. Papers* **79** 2177–89
[38] Khalyavka T O *et al* 2026 Synthesis and characterization of nanostructured Co-Si co-doped TiO_2 with enhanced visible-light photocatalytic performance in phenol red degradation *Ceram. Int.* **52** 1221–36
[39] Phan T D, Vo C M, Tran T M T, Luu T L A and Nguyen X S 2019 Structural and bandgap properties of titanium dioxide nanotube/graphene oxide composites prepared by a facile hydrothermal method *Mater. Res. Express* **6** 105054
[40] Klein J, Kampermann L, Mockenhaupt B, Behrens M, Strunk J and Bacher G 2023 Limitations of the Tauc plot method *Adv. Funct. Mater.* **33** 2304523